Investigation of Demagnetization Effect in an Interior V-Shaped Magnet Synchronous Motor at Dynamic and Static Conditions

F. Mahmouditabar*, A. Vahedi*(C.A.) and P. Ojaghlu*

Abstract: Permanent magnet motors have been considered for a variety of applications due to their features such as high power density and high efficiency. One of the issues that should be investigated in the design of these motors is the demagnetization problem. Usually, the demagnetization analysis is carried out in a steady state, while demagnetization effect in dynamic condition is more considerable due to pulse shaped of armature field. Based on this fact, in this paper, dynamic demagnetization is investigated for an IPM V-shaped magnet. This study has been done for two types of magnet, each one in static & dynamic conditions and the results are compared. Moreover, the effect of flux weakening regime on demagnetization is investigated.

1 Introduction

CONSUMPTION interior permanent magnet motors have been widely recognized for its excellent performance, high efficiency, high power density and high reliability in recent years, and are widely used in industries, tensile engines and home applications [2], [3]. One of the problems with this type of permanent magnet motor is related to its demagnetization, which is caused by conditions such as strong magnetic field, high working temperature, self-demagnetization, high mechanical stress, or a combination of these factors [4], [5]. This phenomenon affects the motor performance characteristics such as power density, output torque, and it also makes torque ripple be increased. Consequently, the machine does not work in ideal design conditions [4,6,7]. So far, little effort has been made in relation to the experimental methods of demagnetizing testing because of its high cost of performing demagnetization

tests in permanent magnet machines, and subsequently losing some of its magnet properties, which leads motor to be permanently damaged [8]. For this purpose, in recent years, several investigations have been made to consider this phenomenon using analytical and simulation methods including the use of an equivalent magnetic circuit [9], reluctance network analysis [10], an analytical method using Poisson equations and boundary conditions [11] and Finite Element Method [12-14].

In this paper, we examine the finite element analysis and Flux 2D software to investigate the demagnetization in a permanent magnet machine, which has the highest accuracy among the existing methods. The basis for the demagnetization is briefly discussed in Section 2. In Section 3, the characteristics of the motor studied and the FEM model of the motor are presented. In Section 4.1, the phenomenon of demagnetization in dynamic and steady-state conditions are investigated using the FEM tool for two types of NdFeB and SmCo magnets. In Section 5 the effect of working in flux weakening region is carried out. Finally, Conclusions are summarized in section 6.

2 The Basis of Demagnetization

This section provides an overview of the basis of

demagnetization in the permanent magnet. The demagnetization phenomenon depends more on the armature reactions, especially in cases where high torque is required. During normal operation of the permanent magnet, the electric current of the stator windings produces a magnetic field in the opposite direction of magnetization in the permanent magnet, which causes demagnetization to occur in the magnet, this can occur in local or in general [15].

As shown in Fig. 1, if the operation point of the magnet is placed above the knee point, only a reversible demagnetization can occur, and after removing the external field, the residual magnetic flux density can be restored [16]. At the lower point of the knee, the density of the magnetic flux density decreases dramatically with the increase of the external field [8]. Now, if the working point is lower than the knee point, the magnet will not go through the previous path and will return to the line called the recoil line. All the recoil lines will have the same slope as the normal curve on the top of the knee point [16]. For this reason, with the removal of the external magnetic field, the residual magnetic flux density will be lower than the initial value. This will weaken the performance of the motor [17].

Fig. 2 shows the normal curve and intrinsic curve of the NdFeB magnet. The intrinsic curve shows only the magnetic field of the magnet, while the normal curve shows the sum of the magnetic field of the magnet and the applied field [8]. Both curves are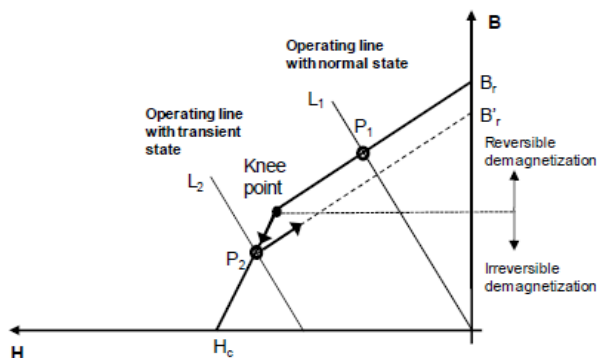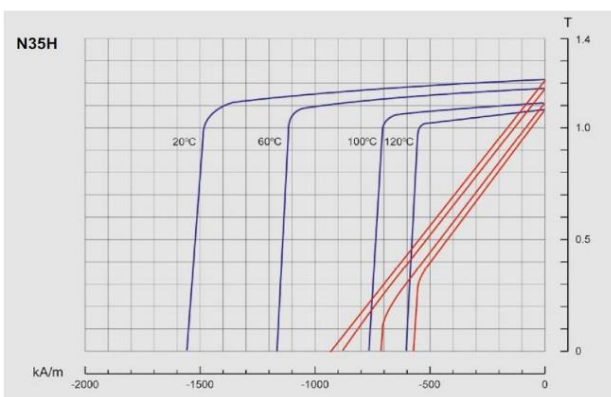 used in demagnetization analysis. When the entire magnet is exposed to a uniform demagnetization field, the normal curve can be used directly to check demagnetization, but in most cases, the magnet is exposed non-uniformly to the demagnetization field; in this case, an intrinsic curve should be used for demagnetizing analysis [8].

Fig. 2 shows the demagnetization curve of the NdFeB magnet used in the IPM machine, which has been shown at various temperatures and it is similar to the SmCo demagnetization curve. Regarding the mentioned curves, we need to study demagnetization at the worst temperature conditions with the highest working temperature of the magnet.

3 IPM Analyzed

The studied device, a brushless AC embedded PM motor presented in Fig. 3, includes the following elements:
1. A fixed part (stator) including yoke, slots, and windings;
2. An air gap;
3. A movable part (rotor) with embedded magnets.

A section of the studied device's model is presented in Fig. 3.

4 FEM Simulations

In the finite element method, the main field problem is divided into a number of subdomains or elements. Then,
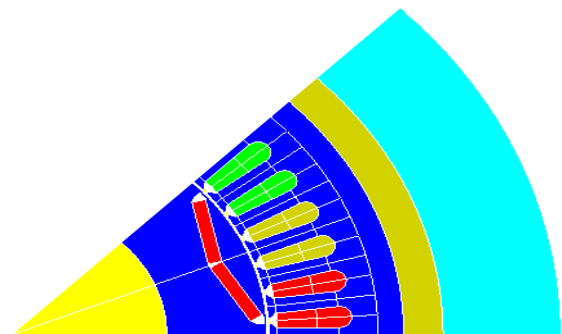
Fig. 1 Calculation of demagnetization point [1].

Fig. 2 demagnetization curve of NdFeB.

Fig. 3 A section of studied IPM motor in Flux 2D.

Table 1 Geometric parameters and materials of IPM analyzed.

Parameter	Value
Max bus voltage	500 (v)
Nominal speed	1200 (rpm)
Nominal current	200 (A)
Air gap	0.6 (mm)
Shaft radius	56 (mm)
Thickness of magnet	5 (mm)
Magnet pole arc	140
Magnet width	54 (mm)
Bridge	1 (mm)
Depth of pole cap	10
Number of pole pairs	4
Rotor external radius	92 (mm)
Number of slots	48
Stator outer radius	141 (mm)
Stack length	75 (mm)

the potential distribution in each element is estimated by a polynomial called (test function), and then a numerical solution for the field problem is obtained from an optimal criterion [18]. Today, the use of finite element method for numerical solution of electromagnetic equations is done by fast, powerful and general-purpose software. In this paper, Flux 2D software is used. Geometric parameters and materials of IPM analyzed presented in Table 1.

4.1 Dynamic State

4.1.1 Armature Reaction

To study the demagnetization in the permanent magnet, which is caused by armature reaction, the IPM machine is studied under the condition that the magnets are not magnetized.

According to Fig. 4, it is shown that the direction of the armature reaction in the left magnet is in some places opposite to the magnetization of the magnet, which causes the magnitude of the flux density in this zone to be lower than the other points.
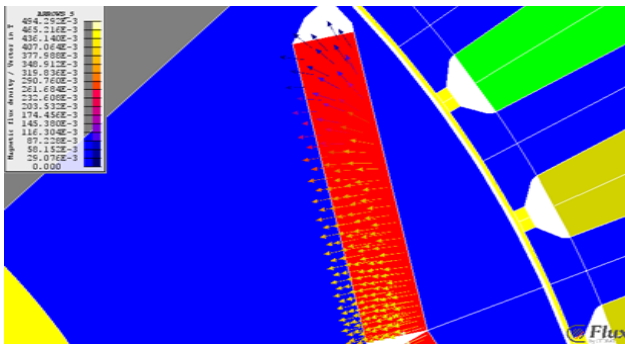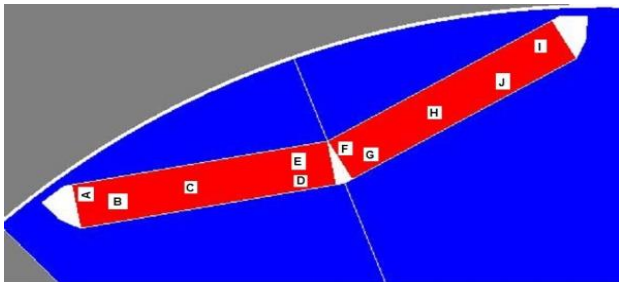

Fig. 4 Direction of armature reaction.
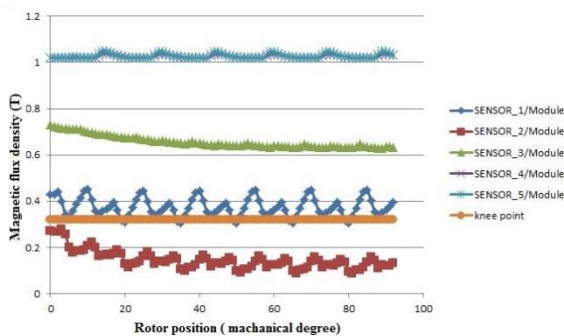

Fig. 5 Position of sensors on magnet.

Fig. 6 Magnetic flux density in left magnet.

4.1.2 Overall Demagnetization in NdFeB Magnet

For a local demagnetization analysis, six points are considered at the magnet surface as shown in Fig. 5. By studying the variations in the flux density of these magnet points in terms of the position of the rotor and the comparison with the magnetic flux density of the knee point at the highest working temperature, investigate of demagnetization phenomenon is carried out.

Looking at the curves and the fluctuation lines presented in Fig. 6 caused by the armature reaction, it can be said that in left magnet at point B, the magnitude of the magnetic flux density in all rotor positions goes down to less than the knee point, which is the demagnetization threshold, and this fact leads the magnet to be demagnetized. The E point also in some of the rotor positions is placed below the knee point, where the worst case occurs in the 82° rotor position and shows partial demagnetization. But in other parts, the flux density is higher than the knee point and the demagnetization does not occur. The reason for demagnetization in these areas is an armature reaction that is in the opposite direction to magnet magnetization, which indicates the demagnetization phenomenon in this magnet.

In the right magnet, as shown in Fig. 7, the flux density at all points are located above the knee point, and even in some places, The measured flux density is larger than magnet residual flux density. This is due to the alignment of the armature reaction and the direction of magnetization of the magnet, which results in increased magnetic flux density and amplification.

The marked blue-bolded parts in Fig. 8 represent a bulk of the magnet having a lower density than the knee point and local irreversible demagnetization has occurred. After calculating, this volume of the magnet is 8.9% of the total magnet volume.
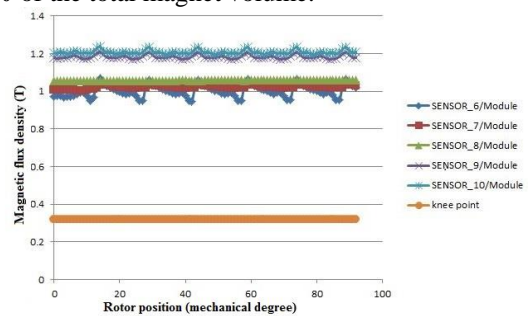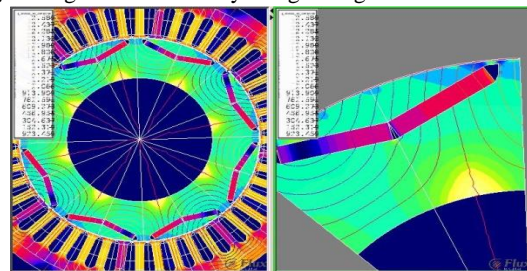

Fig. 7 Magnetic flux density in right magnet.

Fig. 8 Demagnetization area.

4.1.3 Overall Demagnetization in SmCo Magnet

This time, after going through all of the above steps for the SmCo Magnet, the endurance of this type of magnet to the demagnetization field is investigated.

By analyzing the results obtained from the FEM simulation as shown in Fig. 9. The percentage of demagnetization is 3.95%, which is lower than the NdFeB magnet, indicating the permanent magnet SmCo's having a higher demagnetization tolerance than NdFeB due to SmCo's higher thermal coefficient Coercive force than NdFeB's.

4.2 Steady State

In this section, simulations are performed for the motor's steady-state condition. The following results are obtained from the demagnetization of two NdFeB and SmCo magnets.

As shown in Fig. 10, the NdFeB demagnetization in the steady state is 3.92%, which is much lower than the dynamic (8.9%). As a result, the risk of demagnetization in dynamic condition is more than the steady state condition.

For the SmCo magnet, according to Fig. 11, the SmCo demagnetization level is 2.94% in the steady state, which is less than the dynamic (3.95%). The results show that the demagnetization analysis should be carried out in the dynamic condition where the external demagnetization field is stronger.

5 Demagnetization Characteristic in Flux Weakening Region

In all electric motors to operate at higher speeds than the rated speed, it is necessary to reduce the rotor flux due to the limitations of the maximum voltage. But in permanent magnet motors, since the rotor flux is generated by a permanent magnet, it is uncontrollable. In practice, to reduce the flux produced by the rotor magnet, the d-axis current of the rotor is used to maintain the motor's voltage within the range [19], [20]. The motor speed torque characteristic for performance in the area below the base speed and above is given in Fig. 12. At the speeds below, the motor speed is fixed at 377.285 Nm. As the motor speeds up to 1200 rpm, the electromagnetic torque of the motor drops and the motor enters the power constant region, which is known to be the flux weakening region.

The Time Stepping Finite Element Method (TSFEM) is used to check the motor's demagnetization in the flux-weakening region. In this method, at each step of the calculation, the magnitude of the flux density of the work point of the various elements of the magnet is compared with the magnetic flux density of the knee point. If the flux density of the working is higher than the knee point, it indicates a reversible demagnetization. In these conditions, the initial residual flux density is used in the next step of the calculation. If the flux density of the working point is lower than magnetic flux density of the knee point, an irreversible demagnetization will occur. In these conditions, the modified residual flux density obtained from the recoil line should be used in the next step of the calculation.

The results of the demagnetization analysis at two speeds in the flux weakening region (constant power) are shown in Fig. 13. The Figs 13a and 13b are shown the electromagnetic curve of the IPM motor at 1500rpm and 1800rpm respectively. It obvious that considering demagnetization gives the better understanding of actual motor performance. By investigating the demagnetization of an NdFeB magnet in the flux
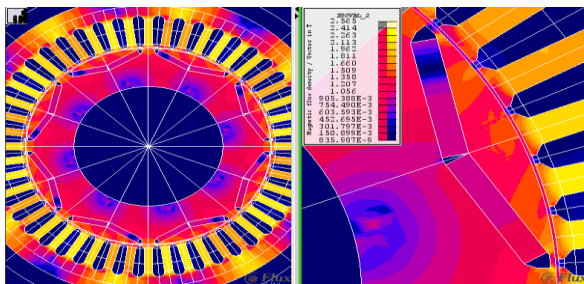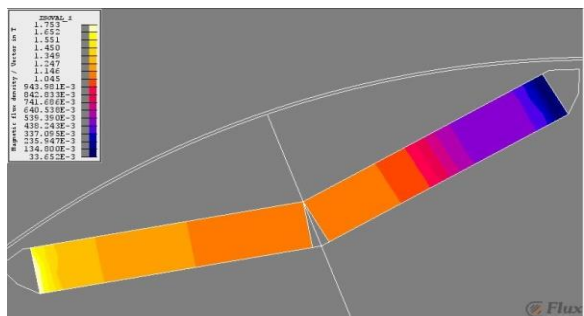

Fig. 9 Demagnetization analysis of SmCo.
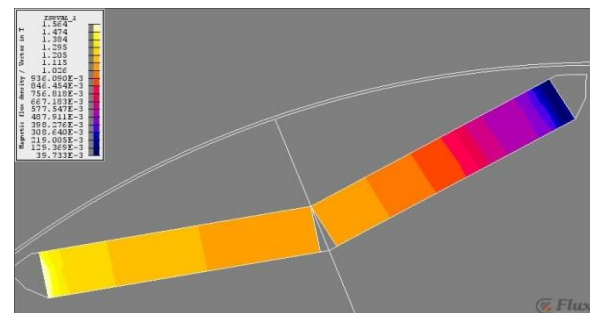

Fig. 11 Demagnetization in dynamic state for SmCo.

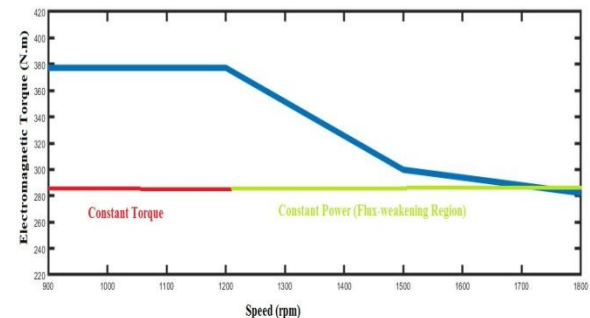**Fig. 10** Demagnetization in steady state for NdFeB.

Fig. 12 Flux-weakening region.

weakening region at 120 °C, the demagnetization level of the magnet at 1500 rpm and 1800 rpm are 17.55% and 18.17% respectively. These results indicate that in flux weakening region as the speed increases, the demagnetization level on the surface of the magnet is increased. The reason for this can be attributed to the d-axis negative polarities current, which produces magnetism in the opposite direction of magnetization of the magnet and causes further demagnetization of the motor.

6 Conclusions

2D FEM analysis is applied in order to investigate the demagnetization phenomenon in IPM V-shaped magnet in dynamic and static conditions. Two types of NdFeB and SmCo magnet materials have been used in this simulation. By analyzing the simulation results, it has been found that demagnetization level for NdFeB in dynamic condition is 8.9%, while it is 3.92% in the steady state, which is significantly lower. For the SmCo Magnet, the percentage of demagnetization has dropped from 3.95% to 2.94%. The results indicate that demagnetization analysis should be studied in the worst condition case that is a dynamic condition with pulsed armature field. It is also found that the NdFeB magnet has less demagnetization tolerance than SmCo due to

(a)

(b)

Fig. 13 Comparison of electromagnetic torque with considering demagnetization and neglecting it at different speeds: a) 1500 rpm, and b) 1800 rpm.

the higher thermal coefficient coercive force in comparison with it. In addition, the negative effect of working in the flux weakening region on demagnetization was investigated. These results indicate that in flux weakening region as the speed increases, the demagnetization level is increased.

References

[1] C. M. Kim, G. W. Cho, G. T. Kim, and H. G. Shin, "The design of flux barrier for improvement of demagnetization endurance in BLDC Motor," *International Conference on Electrical Machines and Systems (ICEMS)*, Busan, pp. 1198–1201, 2013.

[2] G. Choi and T. M. Jahns, "Demagnetization characteristics of permanent magnet synchronous machines," *IECON 2014 - 40th Annual Conference of the IEEE Industrial Electronics Society*, Dallas, TX, pp. 469–475, 2014.

[3] V. I. Patel, J. Wang, and S. S. Nair, "Demagnetization Assessment of Fractional-Slot and Distributed Wound 6-Phase Permanent Magnet Machines," *IEEE Transactions on Magnetics*, Vol. 51, No. 6, pp. 1–11, Jun. 2015.

[4] K. S. Kim, K. S. Kim, B. H. Lee, and B. H. Lee, "Design of concentrated flux synchronous motor to prevent irreversible demagnetization," *IEEE International Electric Machines and Drives Conference (IEMDC)*, Miami, FL, USA, pp. 1–6, 2017.

[5] J. R. Riba Ruiz, J. A. Rosero, A. Garcia Espinosa, and L. Romeral, "Detection of Demagnetization Faults in Permanent-Magnet Synchronous Motors Under Nonstationary Conditions," *IEEE Transactions on Magnetics*, Vol. 45, No. 7, pp. 2961–2969, Jul. 2009.

[6] H. K. Kim and J. Hur, "Dynamic Characteristic Analysis of Irreversible Demagnetization in SPM- and IPM-Type BLDC Motors," *IEEE Transactions on Industry Applications*, Vol. 53, No. 2, pp. 982–990, 2017.

[7] D. H. Kang, H. K. Kim, and J. Hur, "Irreversible demagnetization diagnosis of IPM-type BLDC motor using BEMF harmonic characteristics based on space harmonics," *IEEE Energy Conversion Congress and Exposition (ECCE)*, Montreal, QC, pp. 6956–6961, 2015.

[8] H. Xiong, J. Zhang, M. W. Degner, C. Rong, F. Liang and W. Li, "Permanent-Magnet Demagnetization Design and Validation," *IEEE Transactions on Industry Applications*, Vol. 52, No. 4, pp. 2961–2970, 2016.
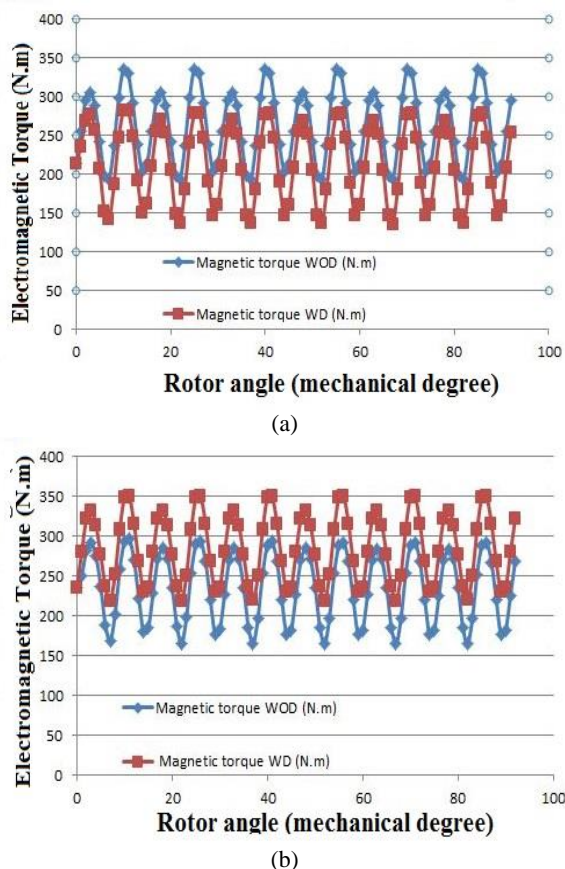
[9] M. Niazazari, M. Mirsalim, and S. Mohammadi, "Analytical framework for analysis and demagnetization study of a slotted solid-rotor line-start permanent-magnet synchronous motor," *The 5th Annual International Power Electronics, Drive Systems, and Technologies Conference (PEDSTC 2014)*, Tehran, pp. 494–499, 2014.

[10] D. Momma, Y. Yoshida, and K. Tajima, "Demagnetization analysis of ferrite magnet motor based on reluctance network analysis," *19th International Conference on Electrical Machines and Systems (ICEMS)*, Chiba, pp. 1–4, 2016.

[11] J. De Bisschop, P. Sergeant, A. Hemeida, H. Vansompel, and L. Dupré, "Analytical Model for Combined Study of Magnet Demagnetization and Eccentricity Defects in Axial Flux Permanent Magnet Synchronous Machines," *IEEE Transactions on Magnetics*, Vol. 53, No. 9, pp. 1–12, Sep. 2017.

[12] W. N. Fu and S. L. Ho, "Dynamic Demagnetization Computation of Permanent Magnet Motors Using Finite Element Method With Normal Magnetization Curves," *IEEE Transactions on Applied Superconductivity*, Vol. 20, No. 3, pp. 851–855, Jun. 2010.

[13] J. H. Park, H. K. Kim, S. T. Lee, and J. Hur, "Characteristics of irreversible demagnetization in accordance with phase advance angle in IPM-type BLDC motor," *IEEE Conference on Electromagnetic Field Computation (CEFC)*, Miami, FL, pp. 1–1, 2016.

[14] K. C. Kim, K. Kim, H. J. Kim, and J. Lee, "Demagnetization Analysis of Permanent Magnets According to Rotor Types of Interior Permanent Magnet Synchronous Motor," *IEEE Transactions on Magnetics*, Vol. 45, No. 6, pp. 2799–2802, Jun. 2009.

[15] P. Peng et al., "Effects of External Field Orientation on Permanent Magnet Demagnetization," *IEEE Transactions on Industry Applications*, Vol. 53, No. 4, pp. 3438–3446, 2017.

[16] R. Fratila, A. Benabou, A. Tounzi, and J. C. Mipo, "Nonlinear Modeling of Magnetization Loss in Permanent Magnets," *IEEE Transactions on Magnetics*, Vol. 48, No. 11, pp. 2957–2960, Nov. 2012.

[17] X. Tang and X. Wang, "Research of the demagnetization mechanism of line-start permanent magnet synchronous motor under the operating condition of sudden reversal," *17th International Conference on Electrical Machines and Systems (ICEMS)*, Hangzhou, pp. 1981–1984, 2014.

[18] E. S. Hamdi, Design of Small Electrical Machines, John Wiley & Sons, 1994, pp. 152–158.

[19] Y. Zhang, L. Xu, M. K. Gven, S. Chi and M. Illindala, "Experimental Verification of Deep Field Weakening Operation of a 50-kW IPM Machine by Using Single Current Regulator," *IEEE Transactions on Industry Applications*, Vol. 47, No. 1, pp. 128–133, 2011.

[20] N. Zhao and N. Schofield, "Field-Weakening Capability of Interior Permanent-Magnet Machines With Salient Pole Shoe Rotors," *IEEE Transactions on Magnetics*, Vol. 53, No. 11, pp. 1–7, Nov. 2017.

F. Mahmouditabar received his BSc in power electrical engineering in August 2016 from Shahrekord University. He is currently working toward his MSc at Iran University of Science and Technology. His research interests include design, modelling and FEA of electrical machines.

A. Vahedi was born in Tehran, Iran, in 1966. He received the B.S. degree from Ferdowsi Mashhad University, Mashhad, Iran, in 1989, and the M.S. and PhD degrees from Institut National Polytechnique de Lorraine (INPL), Nancy, France, in 1992 and 1996, respectively, all in electrical engineering.
He is currently a Professor at Iran University of Science and Technology, Tehran, Iran, where he is a member of the Center of Excellence for power system Automation and Operation, Department of Electrical Engineering.

P. Ojaghlu was born in Zanjan, Iran. He received the B.S. and M.S degrees (with honors) in power electrical engineering in 2010 and 2012, respectively, from Iran University of Science and Technology, Tehran, Iran, where he is currently working toward the PhD degree.
His research interests include design, modelling, optimization and FEA of electrical machines and other electromagnetic devices. Also, he works on the application of power electronics in Variable Frequency Drives (VFDs) and motor control.